

A Flow-based Method for Problems with Vanishing Constraints

Christoph Hansknecht¹, Julian Niederer², and Andreas Potschka¹

¹Institute of Mathematics, Clausthal University of Technology,
Clausthal-Zellerfeld, Germany

²Interdisciplinary Center for Scientific Computing, University of
Heidelberg, Heidelberg, Germany

March 2, 2026

Abstract

Mathematical Programs with Vanishing Constraints (MPVCs) are a notoriously challenging class of problems owing to their lack of constraint qualification. Therefore, to tackle these problems, relaxation-based approaches are typically used. While often yielding satisfactory results, they generally require significant manual tuning and adjustment of the relaxation parameter. To circumvent these problems, we introduce a novel approach based on piecewise gradient flows leading to first-order stationary points. We demonstrate the effectiveness of our method on several real-world MPVC instances and compare it to a common relaxation approach.

1 Introduction

This paper investigates the usefulness of the *Sequential Homotopy Method* [20] for solving so-called *Mathematical Programs with Vanishing Constraints* [1]. These programs, called MPVCs for short are optimization problems of the form

$$\begin{aligned}
 & \min_{x \in C} f(x) \\
 & \text{s.t. } g(x) = 0, \\
 & \quad H_i(x) \geq 0, \quad \text{for } i = 1, \dots, l, \\
 & \quad G_i(x)H_i(x) \geq 0, \quad \text{for } i = 1, \dots, l
 \end{aligned} \tag{MPVC}$$

for functions $f, G_i, H_i : \mathbb{R}^n \rightarrow \mathbb{R}$, and $g : \mathbb{R}^n \rightarrow \mathbb{R}^m$, which we assume to be at least twice continuously differentiable, $C := \{x \in \mathbb{R}^n \mid x_l \leq x \leq x_u\}$ the convex set derived from the (possibly infinite) variable bounds on x .

The difficulty in solving MPVCs arises from the products $G_i(x)H_i(x)$. The constraints G_i are called *vanishing* because, depending on the value of their corresponding *controlling* constraint H_i , G_i is either present in the problem (when $H_i(x) > 0$) or vanishes from it (when $H_i(x) = 0$). Consequently the feasible region of an MPVC decomposes into different pieces where either $H_i(x) > 0$ and $G_i(x) \geq 0$ or $H_i(x) = 0$ and $G_i(x)$ is free. The intersection of these pieces (if it exists) consists of the points x satisfying $G_i(x) \geq 0$ and $H_i(x) = 0$. Following the convention in [1], we define for a feasible point $x \in \mathbb{R}^n$ the following index sets

$$\begin{aligned} \mathcal{I}_{00}(x) &:= \{i \mid H_i(x) = 0, G_i(x) = 0\}, & \mathcal{I}_{+0}(x) &:= \{i \mid H_i(x) > 0, G_i(x) = 0\}, \\ \mathcal{I}_{0+}(x) &:= \{i \mid H_i(x) = 0, G_i(x) > 0\}, & \mathcal{I}_{++}(x) &:= \{i \mid H_i(x) > 0, G_i(x) > 0\}, \\ \mathcal{I}_{0-}(x) &:= \{i \mid H_i(x) = 0, G_i(x) < 0\}, & \mathcal{I}_+(x) &:= \mathcal{I}_{+0}(x) \cup \mathcal{I}_{++}(x), \\ \mathcal{I}_0(x) &:= \mathcal{I}_{00}(x) \cup \mathcal{I}_{0+}(x) \cup \mathcal{I}_{0-}(x), \end{aligned}$$

where we call the indices in $\mathcal{I}_{00}(x)$ and respective constraints *bi-active* (see Figure 1). The reason for the difficulty of solving programs with vanishing

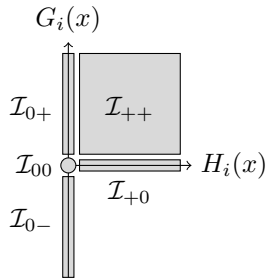


Figure 1: The feasible region of a controlling / vanishing constraint in vertical form.

constraints is the loss of strong constraint qualifications. For instance, the well-known *Linear Independence Constraint Qualification (LICQ)* [18] as well as the slightly weaker *Mangasarian-Fromovitz Constraint Qualification (MFCQ)* [16] are generally not satisfied at bi-active points of MPVCs (see [1] for an in-depth explanation). Consequently, as any nonlinear solver approaches such points, the determination of suitable Lagrange multipliers satisfying the KKT conditions becomes hard or even impossible.

MPVCs are closely related to so-called *Mathematical Programs with Equilibrium Constraints*, called MPECs for short [14], which are identical to MPVCs except for the fact that the products $G_i H_i$ must be zero rather than non-negative. Indeed, MPVCs can be transformed to MPECs by introducing additional slack variables [1, Lemma 1]. The problem class consisting of MPVCs and MPECs is therefore also often referred to as *Mathematical Programs with Complementarity Constraints (MPCCs)*.

From a theoretical view, it is necessary to derive a concept of stationarity in order to obtain practically useful first-order optimality conditions for

MPCCs. Consequently, several different stationarity concepts valid under varying problem-specific constraint qualifications particularly for MPECs have been introduced, such as B-stationarity [5], W- and S-stationarity [21]. These stationarity concepts have great effect on the practical tractability, where weaker stationarity concepts allow for the design of reliably convergent algorithms (see e.g. [4]). In certain applications it is however crucial to obtain points satisfying *strong stationarity* conditions (which we will define later in Theorem 2.1 in Section 2), rendering such approaches useless. One method converging to points satisfying strong stationarity conditions is an SQP method presented in [13].

Another approach to solving generic MPCCs is to artificially introduce regularity by adding a regularization term to the vanishing constraints (see e.g. [8, 11, 12, 19] for a summary). For instance, for MPEC problems a parameter $\sigma > 0$ is chosen, and the equilibrium constraints $G_i H_i = 0$ are replaced by $\Phi(G_i, H_i, \sigma) = 0$, where $\Phi : \mathbb{R} \times \mathbb{R} \times \mathbb{R} \rightarrow \mathbb{R}$ tends to $G_i H_i$ for $\sigma \rightarrow 0$ while satisfying LICQ or MFCQ for $\sigma > 0$. The optimization is then carried out by solving a sequence of NLPs parameterized in σ , which is driven to zero. At each step, the optimal solution of one NLP is used to initialize the next one. A popular regularization function is due to [22], where $\Phi(G_i, H_i, \sigma) = G_i H_i - \sigma$. Regardless of the function however, the relaxation parameter must be carefully selected or adjusted through an iterative process and there remains a risk that exact feasibility is achieved only in the limit as the relaxation parameter tends to zero.

Regardless of the solution approach, it is however often convenient to reformulate MPVCs in order to separate the nonlinear constraints from the combinatorial structure of the feasible set imposed by the vanishing constraints (VC) and controlling constraints (CC). Specifically, by introducing additional (otherwise unconstrained) slack variables, we can ensure that the vanishing and controlling constraints G_i and H_i consist of individual variables, i.e., $G_i(x) = s_{i+l}$ and $H_i(x) = s_i$ for $i + l, i = 1, \dots, n$. We combine the slack variables in the vector $s \in \mathbb{R}^{2l}$. We may require that the slack variable bounds are non-trivial in the sense that the lower bounds $s_l \in \mathbb{R}^{2l}$ are zero at all entries of i and not positive for the entries $i + l$ as well the upper bounds $s_u \in \mathbb{R}^{2l}$ are not negative respectively at all entries. We define $C^s := \{s \in \mathbb{R}^{2l} \mid s_l \leq s \leq s_u\}$ as the convex set of the slack variables. Such a structure of (MPVC) is called its *vertical form*.

$$\begin{aligned}
& \min_{x \in C, s \in C^s} && f(x) \\
& \text{s.t.} && g(x) = 0, \\
& && H_i(x) - s_i = 0, \quad \text{for } i = 1, \dots, l, \\
& && G_i(x) - s_{i+l} = 0, \quad \text{for } i = 1, \dots, l, \\
& && s_i \geq 0, \quad \text{for } i = 1, \dots, l, \\
& && s_{i+l} s_i \geq 0, \quad \text{for } i = 1, \dots, l.
\end{aligned} \tag{MPVCS}$$

Throughout this paper, we will follow an approach similar to [13], consisting of incorporating constraints and their bounds into local subproblems in different

ways, depending on the current index set. However, in our approach, we reduce the complexity by focusing on the biactive points and following actions along the solution path. Specifically, after discussing the theoretical foundations of the problem in Section 2, we will propose a practical algorithm in Section 3, which we base on the concept of gradient flows. After discussing implementational details in Sections 4 and 5, we go on to present numerical results on truss topology design problems in Section 6.

Notation As in [20], we let $\langle x, x' \rangle_X$ be a scalar product inducing the norm $\| \cdot \|_X$ for two points $x, x' \in X$ in a real finite dimensional Hilbert space X . Likewise we get a scalar product real finite dimensional Hilbert spaces Y, \tilde{S} .

2 Constraint Qualifications

We begin by introducing a concept of stationarity in order to obtain practically useful first-order optimality conditions for MPCCs. Specifically, we rely on the MPVC *strong stationarity* concept introduced in [10]. To this end, we let

$$\min \tilde{f}(\tilde{x}) \text{ s.t. } \tilde{g}(\tilde{x}) = 0, \tilde{h}(\tilde{x}) \geq 0 \quad (\text{MPVC-NLP})$$

be (MPVC) as a standard NLP, where $\tilde{f} : \mathbb{R}^{\tilde{n}} \rightarrow \mathbb{R}$, $\tilde{g} : \mathbb{R}^{\tilde{n}} \rightarrow \mathbb{R}^{\tilde{m}}$, and $\tilde{h} : \mathbb{R}^{\tilde{n}} \rightarrow \mathbb{R}^{\tilde{p}}$ and $\tilde{M} := \{x \mid \tilde{g}(\tilde{x}) \leq 0, \tilde{h}(\tilde{x}) = 0\}$ be its set of feasible points. The *linearized cone* [1] of the reformulation at a point $\tilde{x} \in \tilde{M}$ is given by

$$\begin{aligned} L(\tilde{x}) &:= \{d \in \mathbb{R}^{\tilde{n}} \mid \nabla \tilde{g}_i(\tilde{x})d = 0 \text{ for } i = 1, \dots, \tilde{p}, \text{ and} \\ &\quad \nabla \tilde{h}_i(\tilde{x})d \leq 0 \text{ for } i \text{ s.t. } \tilde{h}_i(\tilde{x}) = 0\} \\ &= \{d \in \mathbb{R}^{\tilde{n}} \mid \nabla g_j(\tilde{x})d = 0 \text{ for } j = 1, \dots, m, \\ &\quad \nabla H_i(\tilde{x})d = 0 \text{ for } i \in \mathcal{I}_{0-}(\tilde{x}), \\ &\quad \nabla H_i(\tilde{x})d \leq 0 \text{ for } i \in \mathcal{I}_{00}(\tilde{x}) \cup \mathcal{I}_{0+}(\tilde{x}), \\ &\quad \nabla G_i(\tilde{x})d \leq 0 \text{ for } i \in \mathcal{I}_{+0}(\tilde{x})\} \end{aligned} \quad (1)$$

Furthermore, the *tangent cone* of a set $M \subseteq \mathbb{R}^n$ at $x \in M$ is given by

$$\begin{aligned} T(M, x) &:= \{d \in \mathbb{R}^n \mid \text{there exist sequences } (x_k) \in M, (\lambda_k) \subset \mathbb{R}_{\geq 0} \\ &\quad \text{with } x_k \rightarrow x \text{ and } \lambda_k(x_k - x) \rightarrow d \text{ for } k \rightarrow \infty\} \end{aligned}$$

and the *polar cone* of a cone $M \subseteq \mathbb{R}^{\tilde{n}}$ is given by

$$M^- := \{d \in \mathbb{R}^{\tilde{n}} \mid \langle d, x \rangle \leq 0 \text{ for all } x \in M\},$$

where $\langle \cdot, \cdot \rangle$ denotes the standard scalar product. A point $\tilde{x} \in \tilde{M}$ is said to satisfy the *Guignard Constraint Qualification* (GCQ) [6] iff $T^-(\tilde{M}, \tilde{x}) = L^-(\tilde{x})$. This more geometric condition is significantly weaker than both LICQ and MFCQ and has a good chance to hold in practice (see [9] for a discussion). Based on this constraint qualification the following stationarity condition holds:

Theorem 2.1 (Theorem 2.5 in [10]). *Let x^* be a local minimum of (MPVC) such that GCQ holds at x^* . Then there exist Lagrange multipliers $y^* \in \mathbb{R}^m$, $\eta_H^*, \eta_G^* \in \mathbb{R}^l$ such that*

$$-\nabla_x \mathcal{L}_{\text{MPVC}}(x^*, y^*, \eta_G^*, \eta_H^*) \in T^-(C, x^*),$$

where

$$\mathcal{L}_{\text{MPVC}}(x, y, \eta) := f(x) + \langle y, g(x) \rangle + \sum_{i=1}^l (\eta_H)_i H_i(x) + \sum_{i=1}^l (\eta_G)_i G_i(x)$$

and

$$(\eta_H)_i \begin{cases} = 0 & \text{if } i \in \mathcal{I}_+ \\ \leq 0 & \text{if } i \in \mathcal{I}_{00} \cup \mathcal{I}_{0+} \\ \text{free} & \text{if } i \in \mathcal{I}_{0-} \end{cases} \quad \text{and} \quad (\eta_G)_i \begin{cases} = 0 & \text{if } i \in \mathcal{I}_0 \cup \mathcal{I}_{++} \\ \leq 0 & \text{if } i \in \mathcal{I}_{+0}. \end{cases}$$

3 A Practical Algorithm

Gradient Flows In order to solve MPVCs we examine primal-dual gradient / anti-gradient flows [20]. We will therefore begin by giving an introduction regarding gradient flows and their use in nonlinear programming. For a nonlinear program

$$\min f(x) \text{ s.t. } g(x) = 0, \text{ and } x \in C \quad (\text{NLP})$$

we let $\mathcal{L}(x, y) := f(x) + \langle y, g(x) \rangle_Y$ be its Lagrangian function, and $\mathcal{L}^\rho(x, y) := \mathcal{L}(x, y) + \frac{\rho}{2} \|g(x)\|_Y^2$ its *augmented Lagrangian* for a parameter $\rho \geq 0$. Based on the augmented Lagrangian the *gradient / anti-gradient flow* emanating from the initial values $x_0 \in C$ and $y_0 \in \mathbb{R}^m$ is defined by the following initial value problem for projected differential equations

$$\dot{x}(t) = P_{T(C, x(t))}(-\nabla_x \mathcal{L}^\rho(x(t), y(t))), \text{ and } \dot{y}(t) = \nabla_y \mathcal{L}^\rho(x(t), y(t)), \text{ with } x(0) = x_0, \text{ and } y(0) = y_0.$$

where $P_M(x)$ denotes the $\langle \cdot, \cdot \rangle_X$ -orthogonal projection of x onto the convex set M . We would like to point out that P_M is in general non-differentiable. The projection operator is however *semismooth* [17] with a set-valued derivative in the sense of Clark, enabling the solution of the equations. Furthermore, it was shown in [20] that the equilibrium points of this flow, i.e., those with $\dot{x}(t) = 0$ and $\dot{y}(t) = 0$ are precisely the stationary points of (NLP). Note that the flow is smooth as long as $T(C, x(t))$ stays constant and non-smooth but continuous during changes of the tangent cone, which occur during changes in the active set of the variable bounds constituting C .

To find a stationary point using gradient flows, we solve the initial value problem until such a time where $\dot{x}(t)$ and $\dot{y}(t)$ have been reduced to an acceptable level, or some other convergence criterion is satisfied. In principle, any integration method, such as for example a projected forward Euler method can

be applied to gradient flow problems. However, since gradient / anti-gradient flows tend to be stiff especially for $\rho \gg 1$, an implicit method is preferable in practice. We therefore choose to compute projected backward Euler steps for a step size of $\Delta t > 0$ and a current point $\hat{x} \in C$, $\hat{y} \in \mathbb{R}^m$ by solving the equations

$$x - P_C(\hat{x} - \Delta t \nabla_x \mathcal{L}^\rho(x, y)) = 0, \text{ and } y - \hat{y} - \Delta t \nabla_y \mathcal{L}^\rho(x, y) = 0.$$

The solution of these equations involving the semismooth operator P_C can be carried out using a semismooth Newton (SSN) method [7]. Unfortunately, the use of SSN methods poses its own challenges, in particular due to the fact that these methods are very hard to globalize and suffer from small radii of local convergence. We therefore opt to interpret the projected backward Euler system as a necessary optimality condition of the following regularized variant of (NLP),

$$\begin{aligned} \min_{x \in C, w \in \mathbb{R}^m} \quad & f^\rho(x) + \lambda \left[\frac{1}{2} \|x - \hat{x}\|_X^2 + \frac{1}{2} \|w - \hat{y}\|_Y^2 \right] \\ \text{s.t.} \quad & c(x) + \lambda w = 0 \end{aligned} \tag{Sub-NLP}$$

where $f^\rho(x) := f(x) + \frac{\rho}{2} \|c(x)\|_Y^2$ and $\lambda := 1/\Delta t$ (see [20]). Thus, to compute the step, we can solve this problem with an off-the-shelf NLP solver. The regularization with λ ensures that the problem always satisfies LICQ for all $\lambda > 0$ (under standard assumptions on f , c , and C). We would like to point out that the variable w can in principle be eliminated from the formulation entirely, yielding a box-constrained problem instead. While this approach seems sensible, this reformulation does however greatly increase the nonlinearity of the subproblem. As a result, a significantly larger value of λ is required for regularization, impeding the convergence of the gradient flow itself.

Branch Decomposition In the following, we examine the combinatorial structure of (MPVCS) in vertical form. Clearly, the feasible region with respect to the slack variable constraints $s_{i+l} \geq 0$ and $s_{i+l}s_i \geq 0$ can be decomposed into two *branches*. We define for every pair (s_{i+l}, s_i) of slack variables for $i = 1, \dots, l$, the *branches*

$$\begin{aligned} C_+(i) &:= \{s_i \geq 0 \text{ and } s_{i+l} \geq 0\}, \text{ and} \\ C_0(i) &:= \{s_i = 0 \text{ and } s_{i+l} \leq 0\}, \end{aligned} \tag{2}$$

where the intersection $C_+(i) \cap C_0(i)$ consists of the biactive points, i.e., $i \in \mathcal{I}_{00}(x)$ for $H_i(x)$ and $G_i(x)$. We call $C_+(i)$ the *upper branch* and $C_0(i)$ the *lower branch*. It is clear that we can always modify an instance to ensure that these conditions are met.

The feasible region for the slack variables of (MPVCS) can be decomposed into a number of convex pieces based on the individual branches. Specifically, for a *signature* $\sigma \in \{0, 1\}^l$, we can set

$$C^b(\sigma) := C^s \cap \left(\bigtimes_{i=1}^l \begin{cases} C_+(i) & \text{if } \sigma_i = 1 \\ C_0(i) & \text{if } \sigma_i = 0, \end{cases} \right)$$

to be the convex piece associated with σ . For this piece, we can investigate the optimization problem

$$\begin{aligned}
& \min_{x \in C, s \in C^b(\sigma)} f(x) \\
& \text{s.t. } g(x) = 0 \\
& \quad H_i(x) - s_i = 0 \quad \text{for } i = 1, \dots, l \\
& \quad G_i(x) - s_{i+l} = 0 \quad \text{for } i = 1, \dots, l
\end{aligned} \tag{NLP}\sigma$$

over the convex domain C and $C^b(\sigma)$. This optimization problem no longer contains any vanishing constraints, and standard arguments show that local minima must satisfy the stationarity criterion of $-\mathcal{L}(x^*, s^*, y^*) \in T^-(C \times C^b(\sigma), (x^*, s^*))$. As a result, we could try to solve (MPVCS) by enumerating over its convex pieces of slack variables while solving a nonlinear program for each individual one and checking for stationarity. Of course, the number of 2^l pieces makes such an approach intractable in practice.

It is however worth discussing the relationship between the stationarity criterion for (MPVC) from Theorem 2.1 and its counterpart for (NLP) σ . Since problem (MPVCS) is a reformulation of (MPVC), the Lagrange multipliers of the slack variables in a solution of (MPVCS) coincide with the Lagrange multipliers of vanishing and controlling constraints in (MPVC). We therefore only need to discuss the relationship between the slack variables of (MPVCS) and (NLP) σ . For short we denote $g^{x,*} := -\nabla_x \mathcal{L}(x^*, s^*, y^*) = -\nabla_x \mathcal{L}_{\text{MPVCS}}(x^*, s^*, y^*)$, $g^{s,*} := -\nabla_s \mathcal{L}(x^*, s^*, y^*)$, and $\bar{g}^{s,*} = -\nabla_s \mathcal{L}_{\text{MPVCS}}(x^*, s^*, y^*)$. The equality of the Lagrange gradients $g^{x,*}$ holds by definition of (NLP) σ . Since in both problem formulations (MPVCS) and (NLP) σ the convex set C does not change we only need to examine the j -th component of the respective Lagrangian gradients $g^{s,*}$ for active constraints and given signature σ . The following cases arise:

- If j is part of the slack variables corresponding to H_i and G_i for an $i \in 1, \dots, l$, i.e., $j = i$ or $j = i+l$, such that $C_+(i) \cap C^s \subseteq C^b(\sigma)$. Consequently, i must be in one of the sets \mathcal{I}_{00} , \mathcal{I}_{0+} , \mathcal{I}_{+0} , or \mathcal{I}_{++} . For $j = i$ and $i \in \mathcal{I}_{+0}$ the case is symmetric and we have $(\eta_H)_i = 0$. For $j = i+l$ and $i \in \mathcal{I}_{+0}$, we can observe that $T^-(C \times C^b(\sigma), (x^*, s^*))$ requires the j -th component of $g^{s,*}$ to be non-positive, whereas that component has to be zero in $T^-(C \times C^s, (x^*, s^*))$ due to the non-trivially chosen variables bounds. Since the otherwise unconstrained $(\eta_G)_i$ can be set to any non-positive value, the residuals can be made to coincide. If $j = i+l$ corresponds to the VC G_i and $i \in \mathcal{I}_{0+}$, the corresponding entry of $(\eta_G)_i$ must be zero and $(\eta_H)_i$ greater equal zero and the stationarity residuals again coincide. Thus, the only remaining case occurs for $i \in \mathcal{I}_{00}$: Here, $T^-(C \times C^b(\sigma), (x^*, s^*))$ requires both $g_i^{s,*}$ and $g_{i+l}^{s,*}$ to be non-positive, whereas $T^-(C \times C^s, (x^*, s^*))$ requires $\bar{g}_{i+l}^{s,*}$ to be zero, which is in general not possible. Thus, if $g_j^{s,*} < 0$ and $j = i+l$, the stationary point for (NLP) σ in the current convex piece does not coincide with a stationary point for (MPVCS).
- If j is part of the slack variables corresponding to a vanishing constraint

$i + l$ or controlling constraint i such that $C_0(i) \cap C^s \subseteq C(\sigma)$. The index set of interest is $i \in \mathcal{I}_{00}$: As before we need to have $g_{i+l}^{s,*} = 0$, since $T^-(C \times C^s, (x^*, s^*))$ requires $\bar{g}_{i+l}^{s,*} = 0$. If $g_j^{s,*} > 0$ and $j = i + l$ the stationary point for (NLP σ) in the current convex piece is therefore not stationary for (MPVCS).

Based on these observations it is easy to see that the stationarity criterion for (MPVC) is stricter than that for individual branches in the sense that a stationary point for (MPVC) is stationary for (NLP σ) for all fitting choices of σ , i.e., $s^* \in C^s \cap C^b(\sigma)$, whereas the converse does not hold in general. Furthermore, the sign of $g^{s,*}$ in the direction of the $i + l$ -entries indicates the non-stationarity of the primal-dual variables (x^*, s^*, y^*) .

Piecewise Gradient Flows To solve (MPVC), we begin at an initial guess $x_0 \in C$ and $s_0 \in C^b(\sigma)$ for some signature σ . This point does not need to satisfy the nonlinear constraint g . Based on the set $C \times C^b(\sigma)$ and an initial estimate $y_0 \in \mathbb{R}^m$, we can consider the gradient flow defined by the equations

$$\begin{aligned} (\dot{x}(t), \dot{s}(t)) &= P_{T(C \times C^b(\sigma), (x(t), s(t)))} (-\nabla_{x,s} \mathcal{L}^\rho(x(t), s(t), y(t))), \\ \dot{y}(t) &= \nabla_y \mathcal{L}^\rho(x(t), s(t), y(t)) \text{ with} \\ x(0) &= x_0, \quad s(0) = s_0, \text{ and } y(0) = y_0. \end{aligned}$$

This flow is of course designed to solve problem (NLP σ). However, as discussed earlier, even a stationary point for $C \times C^b(\sigma)$ is not generally going to be a solution of (MPVCS). It is therefore necessary for the flow to leave one convex piece and switch to another while preserving continuity. Of course a continuous switch between the different branches can only be conducted at times $t > 0$ where the slack variables $s(t)$ of the flow becomes bi-active for some i . At such a time, we are free to switch the signature by flipping one or more branches for $i \in \mathcal{I}_{00}(x(t))$ while maintaining continuity (but not smoothness) of the resulting flow, which we combine with a detection of the stationarity of (MPVCS), to prevent the continuation of the flow into any other branch. Thus, for a given primal-dual (x, s, y) with signature σ we start by determining whether the pair is stationary according to the conditions of Theorem 2.1. To this end, the multipliers η_H and η_G are chosen in such a way as to minimize the absolute value of the corresponding components of $g_{\text{MPVCS}} := -\nabla_{x,s} \mathcal{L}_{\text{MPVCS}}(x, s, y)$ subject to the sign constraints of the multipliers. The stationarity residual is then given by the distance of $g_{\text{MPVCS}} - P_{T^-(C \times C^s, (x^*, s^*))}(g_{\text{MPVCS}})$ with respect to an appropriate norm. Once this residual is below some threshold ε , the solution is (approximately) stationary. If stationarity is not achieved, switching candidates are identified using $-\nabla_{x,s} \mathcal{L}^\rho(x, s, y)$, yielding a new signature σ' and updated branches:

- If $i \in \mathcal{I}_{00}(x)$ and $\sigma_i = 1$ we switch to the lower branch $C_0(i)$ if

$$(-\nabla_s \mathcal{L}^\rho(x, s, y))_i \leq 0 \quad \text{and} \quad (-\nabla_s \mathcal{L}^\rho(x, s, y))_{i+l} < 0,$$

which means the slack variable s_{i+l} will vanish. We update the signature by setting $\sigma'_i = 0$.

- If $i \in \mathcal{I}_{00}(x)$ and $\sigma_i = 0$ we switch to the upper branch $C_+(i)$ if

$$(-\nabla_s \mathcal{L}^\rho(x, s, y))_{i+l} > 0,$$

or

$$(-\nabla_s \mathcal{L}^\rho(x, s, y))_{i+l} = 0 \quad \text{and} \quad (-\nabla_s \mathcal{L}^\rho(x, s, y))_i > 0,$$

which means the slack variable s_{i+l} is free in the next piece of the gradient flow. We update the signature by setting $\sigma'_i = 1$.

- The bounds and signature values of all other variables are kept constant.

Once σ' has been chosen, we continue with the next piece of our piecewise gradient flow at the point (x, s, y) (with $(x, s) \in C \times C^b(\sigma')$) and integrate along the signature-modified initial value problem by setting

$$\begin{aligned} (\dot{x}(t), \dot{s}(t)) &= P_{T(C \times C^b(\sigma'), (x(t), s(t)))} (-\nabla_{x,s} \mathcal{L}^\rho(x(t), s(t), y(t))), \\ \dot{y}(t) &= \nabla_y \mathcal{L}^\rho(x(t), s(t), y(t)) \quad \text{with} \\ x(0) &= x, \quad s(0) = s, \quad \text{and} \quad y(0) = y. \end{aligned}$$

Note, $\dot{y}(t)$ is independent of the choice of signatures and remains unchanged.

4 Implementational Aspects

In the following, we discuss some aspects of the implementation required for the solution of particularly challenging instances.

Algorithmic Parameters The choice of the algorithmic parameters λ and ρ has a large impact on the convergence speed of our method. The parameter λ (the inverse of the step size Δt) controls the progress of the gradient / anti-gradient flow towards stationary points. Thus, we would like to decrease λ as far as possible. However, if the risk of ill-conditioned (Sub-NLP) increases. To prevent divergence of subsystem solvers, we propose a simple heuristic to update λ after each iteration: Based on an initial value of $\lambda^{(0)} = \lambda_{\text{init}}$, we set

$$\lambda^{(k+1)} := \begin{cases} \lambda_{\text{inc}}^{-1} \cdot \lambda^{(k)} & \text{if current (Sub-NLP) was solved successfully} \\ \lambda_{\text{inc}} \cdot \lambda^{(k)} & \text{otherwise,} \end{cases}$$

where we set $\lambda_{\text{init}} = 0.1$ and $\lambda_{\text{inc}} = 2$.

In contrast to the value of λ , the method is less dependent on the choice of the parameter ρ . In many cases, a small constant value of ρ is sufficient. As an alternative, we propose a simple rule to update ρ which works by ensuring that,

whenever possible, the value $\frac{1}{2}\|c(x(t))\|^2$ is non-increasing along the trajectory. To ensure this property, we note that

$$\frac{d}{dt} \frac{1}{2} \|c(x(t))\|^2 = -\langle d, P'(\nabla f(x(t)) + y(t)^T J_c(x(t))) \rangle - \rho \langle d, P'd \rangle$$

where $d := c(x(t))^T J_c(x(t))$ and $P' \in \mathbb{R}^{n \times n}$ is an element of the set-valued derivative of the projection operator P . Consequently, as long as $\langle d, P'd \rangle < 0$ we can increase ρ sufficiently in order to ensure that $\frac{1}{2}\|c(x(t))\|^2$ does not increase. In practice, our approach is more conservative and we increase ρ at most by a factor of $\rho_{\text{inc}} = 10$ per iteration.

Scaling The aspect of scaling plays an important role during the implementation of nonlinear programming codes [23, Sec. 3.8], as it can dramatically speed up the convergence on badly scaled real-world instances. To include scaling in our algorithm, we employ the scalar products $\langle \cdot, \cdot \rangle_X$ and $\langle \cdot, \cdot \rangle_Y$ whose induced norms appear in (Sub-NLP). Since the stationarity conditions are independent of the underlying norm of the space, we are free to employ these scalar products to improve convergence. Specifically, rather than the standard Euclidean scalar product, it may be convenient to use scalar products induced by scaling matrices D_x , D_s and D_y instead and solve

$$\begin{aligned} \min_{x \in C, s \in C^{\text{b}}(\sigma), w \in \mathbb{R}^m} \quad & f^\rho(x, s) + \lambda \left(\frac{1}{2} (x - \hat{x})^T D_x (x - \hat{x}) \right. \\ & \left. + \frac{1}{2} (s - \hat{s})^T D_s (s - \hat{s}) + \frac{1}{2} (w - \hat{y})^T D_y (w - \hat{y}) \right) \\ \text{s.t.} \quad & c(x, s) + \lambda w = 0 \end{aligned} \quad (3)$$

Furthermore, it can be advantageous to scale the variables itself.

5 Vanishing Constraints

Let us consider an instance of (MPVCS) in vertical form to use this additional structure to realize an efficient implementation.

Initializing Branches To find a suitable branch and feasible starting values for the slack variables we evaluate at a given primal initial guess the controlling and vanishing constraints:

- If $H_i(x) > 0$ we set $s_i = H_i(x)$, $s_{i+l} = \max\{0, G_i(x)\}$ and we choose the branch $C_+(i)$.
- If $H_i(x) = 0$ we set $s_i = 0$, $s_{i+l} = G_i(x)$. Depending on the value s_{i+l} we choose $C_+(i)$ if $s_{i+l} > 0$ and $C_0(i)$ otherwise.
- If $H_i(x) < 0$ we set $s_i = 0$ and choose the lower branch $C_0(i)$ and set $s_{i+l} = \min\{0, G_i(x)\}$.

Reduced Subsequent NLPs Note, that the lower branch C_0 from (2) corresponds to the set of vanishing constraints indexed by \mathcal{I}_{0-} . In this case, the controlling constraints in \mathcal{I}_{0-} are treated as equality constraints. This observation aligns with the structure of the linearized cone presented in (1). More precisely, the vanishing constraints G_i , respectively the slack variables s_{i+l} , for $i \in \mathcal{I}_{0-}$ have vanished from the linearized cone, as they do not contribute to feasibility or optimality conditions at a local minimum. This is also reflected in the zero Lagrange multipliers for the vanishing constraints in \mathcal{I}_{0-} at a strong stationary point. Consequently, these vanished constraints, i.e., the constraints in the lower branch C_0 can be omitted in the formulation of the subsequent NLP. A similar idea can be found in [13]. Let σ be a signature for the branch decomposition. We define the reduced slack variables

$$\tilde{s} := (s_1, \dots, s_i, (s_{i+l}, \text{ for } \sigma_i = 1))^T,$$

with

$$C^r(\sigma) := C^s \cap \left(\bigtimes_{i=1}^l \begin{cases} C_+(i) & \text{if } \sigma_i = 1 \\ \{s_i = 0\} & \text{if } \sigma_i = 0. \end{cases} \right)$$

and respective real Hilbert space \tilde{S} with its induced norm. The reduced constraints are

$$\tilde{c}(x, \tilde{s}) := \begin{pmatrix} g(x) \\ H_i(x) - s_i & \text{for } i = 1, \dots, l \\ G_i(x) - s_{i+l} & \text{for } \sigma_i = 1 \end{pmatrix} \in \mathbb{R}^r$$

with $r = m + l + \#\{i \mid \sigma_i = 1\}$. We consider the following reduced problem:

$$\begin{aligned} \min_{x \in C, \tilde{s} \in C^r(\sigma), \tilde{w} \in \mathbb{R}^r} & \tilde{f}^\rho(x, \tilde{s}) + \lambda \left[\frac{1}{2} \|x - \hat{x}\|_X^2 + \frac{1}{2} \|\tilde{s} - \tilde{\hat{s}}\|_{\tilde{S}}^2 + \frac{1}{2} \|\tilde{w} - \tilde{\hat{y}}\|_Y^2 \right] \\ \text{s.t.} & \tilde{c}(\tilde{x}) + \lambda \tilde{w} = 0, \end{aligned}$$

(Red-NLP)

where \tilde{w} is a vector of the same dimension as \tilde{c} , $\tilde{f}^\rho(x, \tilde{s})$ denotes the reduced augmented objective, and $\tilde{\hat{x}}$, $\tilde{\hat{s}}$, and $\tilde{\hat{y}}$ are the corresponding reduced solutions from the previous iteration.

Following the solution of (Red-NLP), the slack variables s_{i+l} for $\sigma_i = 0$ are updated such that they satisfy $G_i(x) - s_{i+l} = 0$ and projected afterwards onto $C^s \cap C_0(i)$ for $\sigma_i = 0$ to detect potential bi-active points and possible switches. The new value for y is given by $\hat{y} - \tilde{w}$ and for the missing values of the VC in the lower branch with zero. We go on to prove the correctness of this modification:

Theorem 5.1. *A strong stationary point of (MPVCS) is equivalent to an equilibrium point under the proposed strategy based on piecewise flows.*

Proof. Consider to the vertical formulation given in (MPVCS). Subsequent NLPs of the piecewise flow are solved with (Red-NLP) and the described updating strategy. Let (x^*, s^*, y^*) be a strong stationary point of (MPVCS). We

have

$$\begin{aligned} -\nabla_{x,s}\mathcal{L}_{\text{MPVCS}}(x^*, s^*, y^*) &\in T^-(C \times C^s, (x^*, s^*)), \\ g(x^*) &= 0, \\ H_i(x^*) - s_i^* &= 0, \quad \text{for } i = 1, \dots, l \\ G_i(x^*) - s_{i+l}^* &= 0, \quad \text{for } i = 1, \dots, l. \end{aligned}$$

We get a signature σ as described in the branch initialization section from vanishing and controlling constraints and their slack variables. It follows $s^* \in C^{\text{b}}(\sigma) \subseteq C^s$ and since $-\nabla_{x,s}\mathcal{L}_{\text{MPVCS}}^\rho(x^*, s^*, y^*) = -\nabla_{x,s}\mathcal{L}_{\text{MPVCS}}(x^*, s^*, y^*)$ we get

$$\begin{aligned} 0 &= P_{T(C \times C^{\text{b}}(\sigma), (x^*, s^*))}(-\nabla_{x,s}\mathcal{L}^\rho(x^*, s^*, y^*)) = (\dot{x}(t), \dot{s}(t)), \\ 0 &= \nabla_y\mathcal{L}_{\text{MPVCS}}(x^*, s^*, y^*) = \nabla_y\mathcal{L}_{\text{MPVCS}}^\rho(x^*, s^*, y^*) = \dot{y}(t). \end{aligned}$$

Conversely, assume an equilibrium point (x^*, s^*, y^*) , i.e., $\dot{x}(t) = 0, \dot{s}(t) = 0$ and $\dot{y}(t) = 0$. Then,

$$0 = \dot{y}(t) = \begin{pmatrix} g(x^*) \\ H_i(x^*) - s_i^* = 0 \quad \text{for } i = 1, \dots, l \\ G_i(x^*) - s_{i+l}^* = 0 \quad \text{for } i = 1, \dots, l. \end{pmatrix}$$

and therefore $\nabla_{x,s}\mathcal{L}_{\text{MPVCS}}^\rho(x^*, y^*, y^*) = \nabla_{x,s}\mathcal{L}_{\text{MPVCS}}(x^*, s^*, y^*)$. From $\dot{x}(t) = 0$, we obtain $-\nabla_{x,s}\mathcal{L}_{\text{MPVCS}}(x^*, s^*, y^*) \in T^-(C \times C^{\text{b}}(\sigma), (x^*, s^*))$ with signature σ , which was used to solve the last (Red-NLP). By construction we have $C^{\text{b}}(\sigma) \subseteq C^s$. We check the conditions on the Lagrange multipliers for satisfying strong stationarity. Depending on σ_i for $i = 1, \dots, l$ we have the following cases:

- If $\sigma_i = 0$ and $s_{i+l} < 0$ we have $i \in \mathcal{I}_{0-}$. By our strategy the respective Lagrange multiplier for s_{i+l} is zero and for the slack of the controlling constraint s_i free, since the controlling constraint is treated as an equality constraint.
- If $\sigma_i = 0$ and $s_{i+l} = 0$, we have $i \in \mathcal{I}_{00}$. Again the respective Lagrange multiplier for s_{i+l} is zero, but for the slack of the controlling constraint s_i is less than or equal to zero. If the Lagrange multiplier for s_i would be positive we would not terminate, since the controlling constraint becomes inactive and a switch must be performed to the upper branch.
- If $\sigma_i = 1$ and $s_i = s_{i+l} = 0$, we have $i \in \mathcal{I}_{00}$. The Lagrange multiplier for the slack of the vanishing constraint is zero and for the slack of the controlling constraint s_i is less than or equal to zero, otherwise we would not terminate at the biactive point.
- The remaining index sets are \mathcal{I}_{0+} , \mathcal{I}_{+0} , and \mathcal{I}_{++} , which are covered by $\sigma_i = 1$. The Lagrange multipliers match the strong stationarity conditions.

It follows that $-\nabla_{x,s}\mathcal{L}_{\text{MPVCS}}(x^*, s^*, y^*) \in T^-(C \times C^s, (x^*, s^*))$. \square

6 Numerical Experiments

In the following we will demonstrate the effectiveness of our approach on several test instances of MPVCs. While large suites of MPEC benchmark problems, such as `NOSBENCH` [19] and `MacMPEC` [15] are available, there are no larger suites of MPVC benchmark problems, but several problems are available in [8, Sec. 9.5], which we adapt for our purposes. We convert all of these problems to their vertical form and initialize our methods at $x_0 = 0, y_0 = 0$ unless stated otherwise. All experiments were conducted on an `Intel Core i7-14700` clocked at 2.1 GHz with 64 GB RAM based on an implementation in `Python 3.13.5` with `CasADi 3.7.1` [2] and using `Ipopt 3.14.11` [23] as subproblem solver for solving (Red-NLP).

6.1 An Academic Example

We begin by examining the following small academic example in two variables:

$$\begin{aligned} \min_{x \in \mathbb{R}^2} \quad & 4x_1 + 2x_2 \\ \text{s.t.} \quad & x_1 \geq 0 \\ & x_2 \geq 0 \\ & (x_1 + x_2 - 5\sqrt{2})x_1 \geq 0 \\ & (x_1 + x_2 - 5)x_2 \geq 0 \end{aligned}$$

This example has the advantage of being low-dimensional and therefore easy to reason about. As shown in Figure 2, the problem consists of a polyhedron with an attached line segment as well as a single isolated point. It has a local optimum at $\hat{x} := (0, 5)$ at the tip of the line segment as well as a global optimum at $x^* := (0, 0)$ in the isolated point. `Ipopt` for example finds with a suitable initial guess one of these points, but usually converging to the point $\hat{x} := (5\sqrt{2}, 0)$, a corner of the polyhedron where the second controlling constraint turns active. Numerical results of our method are shown in Figure 3. We visualize a flow in Figure 2 starting with $\lambda = 100$ and slightly decreasing by a factor of 1.01. The flow consists of 637 points computed with 4602 `Ipopt` iterations. Note, that we use $\lambda_{\text{init}} = 0.1$ and a decreasing factor of $\lambda_{\text{inc}} = 2.1$ from now on. This results in a convergence in 6 iterations with 37 `Ipopt` iterations of the academic example. Due to the slack variable reformulation a mismatch of the constraints during the solution process depending on the starting point can be observed. Furthermore our method converges from every starting point inside the test region $[-3.75, 11.75] \times [-3.75, 11.75]$ to a minimum (see Figure 3a). The results are comparable to the global relaxation approach in e.g. [11]. Due to the branch initialization process, the regions of convergence differ from the results in [11]. If we put every infeasible pair of controlling and vanishing constraint in the lower branch C_0 , the region of convergence of the global minimum would expand close to the local minimum, but not reaching the feasible set beside the isolated global minimum (see Figure 3b).

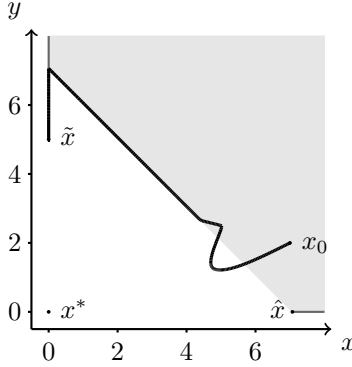


Figure 2: One example flow for the starting point $(7,2)$ is shown in black. The feasible set is marked in grey with active controlling constraints in dark grey, showing the nonconvex structure. The global optimal point is x^* , the local optimal point is \hat{x} , and a further convergence point for standard solver is \hat{x} .

6.2 Truss Topology Optimization

Truss topology optimization problems appear in civil engineering application, where structures are supposed to be designed in such a way as to resist certain external loads without buckling while being attached at certain points and free to flex under loads at others (see [3] for an introduction). Examples of such structures are bridges designed to handle the load of passing vehicles or cantilevers fixed at either end while having a load attached at the other. Truss design problems can be stated as

$$\begin{aligned}
 \min_{a \in \mathbb{R}^N, u \in \mathbb{R}^{Ld}} \quad & \sum_{i=1}^N \ell_i a_i \\
 \text{s.t.} \quad & K(a)u_l = f_l && \text{for all } l = 1, \dots, L \\
 & f_l^T u_l \leq c && \text{for all } l = 1, \dots, L \\
 & 0 \leq a_i \leq \bar{a} && \text{for all } i = 1, \dots, N \\
 & (\bar{\sigma}^2 - \sigma_{il}(a, u)^2) a_i \geq 0 && \text{for all } i = 1, \dots, N, l = 1, \dots, L.
 \end{aligned}$$

Here, the variables a_i denote the cross-sectional area of a set of $N > 0$ potential bars (which are actually present only when $a_i > 0$) connecting a number of points in 2-dimensional space, where each bar has a fixed length of $\ell_i > 0$. Naturally, the area is bounded below by zero and above by some constant $\bar{a} > 0$. The objective of the problem is to reduce the amount of material required by the truss, which is proportional to the sum of volumes over all bars.

As mentioned above, the designed structure is supposed to resist external loads. Specifically, there are $L \in \mathbb{N}$ load cases, during each of which a load exerts forces on a subset of the points. The points themselves fall into two categories: They are either fixed points at which the structure is attached, or

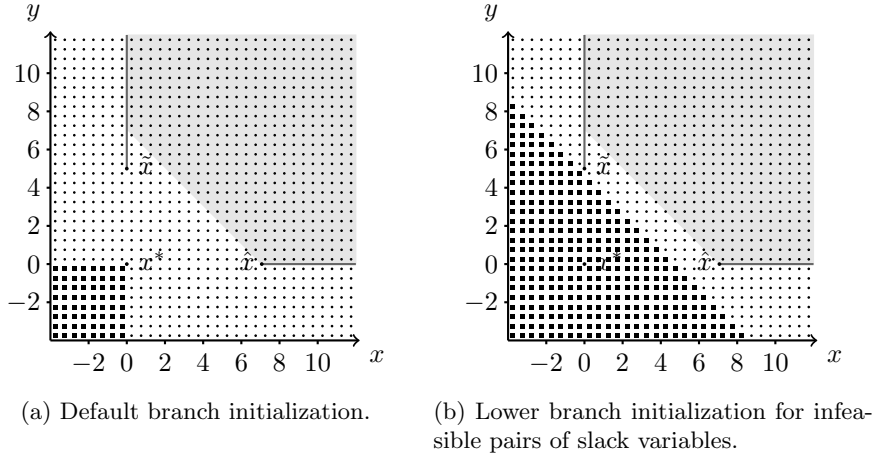


Figure 3: Numerical results for the academic example. The feasible set is marked in grey with active controlling constraints in dark grey. The global optimal point is x^* , the local optimal point is \tilde{x} , and a further convergence point for standard solver is \hat{x} . Starting points where our method converges to the local optimum is shown with circles. Rectangles mark the convergence of our method to the global minimum. Figure (a) shows the convergence regions with the prescribed branch initialization strategy. Figure (b) shows the convergence regions, if every infeasible pair of slack variables is initialized in the lower branch.

they are free points at which a load case may cause a non-zero displacement. The displacements of the latter points under different load cases are contained in the variables $u = (u_1, \dots, u_L)$, where we let $d \in \mathbb{N}$ be the total dimension of each u_l , given by the product of the number of free points and the ambient dimension of 2. The matrix

$$K(a) := \sum_{i=1}^N a_i \frac{E}{\ell_i} \gamma_i \gamma_i^T$$

is the global stiffness matrix of the problem with a fixed value E for Young's modulus and vectors $\gamma_i \in \mathbb{R}^d$ containing the cosines of the angles between the displacement coordinate and bar axes. The equations $K(a)u_l = f_l$ then model equilibrium conditions, where each vector $f_l \in \mathbb{R}^d$ contains the external loading force applied to the free points, while the inequalities $f_l^T u_l \leq c$ bound the compliance of the structure by another constant $c > 0$. Finally, the structure must obey the *stress constraint*, stating that the absolute value of the stress

$$\sigma_{il}(a, u) := E \frac{\gamma_i^T u_l}{\ell_i}$$

should be bounded above by a constant $\bar{\sigma} > 0$. This condition is squared to remove the absolute value. The constraint is however only required when

a bar is actually present (i.e., $a_i > 0$) and redundant otherwise. Hence, it is formulated as a vanishing constraint controlled by the value of a_i . We would like to point out all of our instances are normalized by setting $E \equiv 1$ and $\|f_\ell\|_2 = 1$. Problems are listed in Table 1 with their solutions in Table 3.

Table 1: List of problem instances with sizes and parameters. Note that the number of VCs corresponds to the number of bars.

Problem	#Vars	#Cons	#VC	\bar{a}	c	$\bar{\sigma}$
TenBar	29	19	10	100	10	1.0
Cant1	497	273	224	1	100	100.0
Cant2	497	273	224	1	100	2.2
Hook1	1 417	756	661	100	100	100.0
Hook2	1 417	756	661	100	100	3.5
Hook3	1 417	756	661	100	100	3.0

Initialization Due to the large number of vanishing constraints being present in truss topology problems, an initialization of zero places the initial point of the flow in a position where all vanishing constraints are bi-active while being far away from stationarity, causing the flow to enter a branch constrained by many variables fixed to zero. We find it to be more advantageous to instead start the optimization at a point bounded away from zero in the upper branch of the problem. To this end, we set $a_i \equiv \alpha$ for all i with a constant $\alpha > 0$. Based on this choice of α , we want u_l to be close to $\arg \min_{u \in \mathbb{R}^d} \|K(a)u - f_l\|$ in order to reduce the residual of the corresponding constraint. In our examples, $K(1)$ is always invertible and we can choose $u_l := \alpha^{-1}K(1)^{-1}f_l$. To ensure that the compliance bound is met, we need that $\alpha \geq c^{-1}f_l^T K(1)^{-1}f_l$ for all load cases. Similarly, for the stress constraint, we need that

$$\frac{\gamma_i^T K(1)^{-1} f_l}{\ell_i \bar{\sigma}} \leq \alpha \quad \text{for all } i = 1, \dots, N, l = 1, \dots, L.$$

By taking the maximum of all these bounds we obtain an α such that the resulting values of a and u yield a solution in the upper branch, which is feasible under the mild assumption that the resulting values of a are all bounded above by \bar{a} .

To compute a dual estimation based on a given primal for a given instance of (MPVCS), we conduct the following steps: First, we compute the signature σ compatible with the primal solution. Second, we consider the corresponding problem (NLP σ) and compute a dual solution minimizing its KKT residuum $\|f(x) + (y, y_s)^T J_g(x, s)\|_2$ while maintaining bounds on y_s compatible with the active set, i.e., forcing entries of y_s to be equal to zero for inactive variables and to be non-negative or non-positive, depending on the active bounds, otherwise. The resulting box-constrained quadratic program can be quickly solved using standard methods, yielding a reasonable initial dual solution y .

Algorithmic settings The parameters $\rho = 10^{-2}$, $\lambda_{\text{init}} = 0.1$, $\lambda_{\text{inc}} = 2.1$ were selected for the calculation of all results. Unless otherwise specified, the variables are scaled before using (Red-NLP), so that all primal and dual variables with an absolute value greater than 1 are scaled to unity in every iteration and the scalar products are not scaled.

6.2.1 Ten-bar Truss

As the first truss design problem we consider the so-called *ten-bar* problem from [8] shown in Figure 4a. It consists of ten potential bars to be placed between six points, two of which being fixed to a wall and a loading force pointing downwards. We set the parameters to $(\bar{a}, c, \bar{\sigma}) = (100.0, 10.0, 1.0)$.

Based on the primal-dual initialization given above, our method converges in 7 iterations with 181 `Ipopt` iterations within less than a second with an optimal volume $V^* = 8.0$. The resulting solution is shown in Figure 4b with individual solution values being shown in Table 2. Note that there is no active compliance constraint, but several feasible stress constraints $\sigma_i^2 \leq \bar{\sigma}^2$, which differs from the solution structure seen in [8], while the optimal volume of our solution does coincide with that in [11]. The value of the compliance constraint and the values of the a_i (with reordering) coincide with the results in [4].

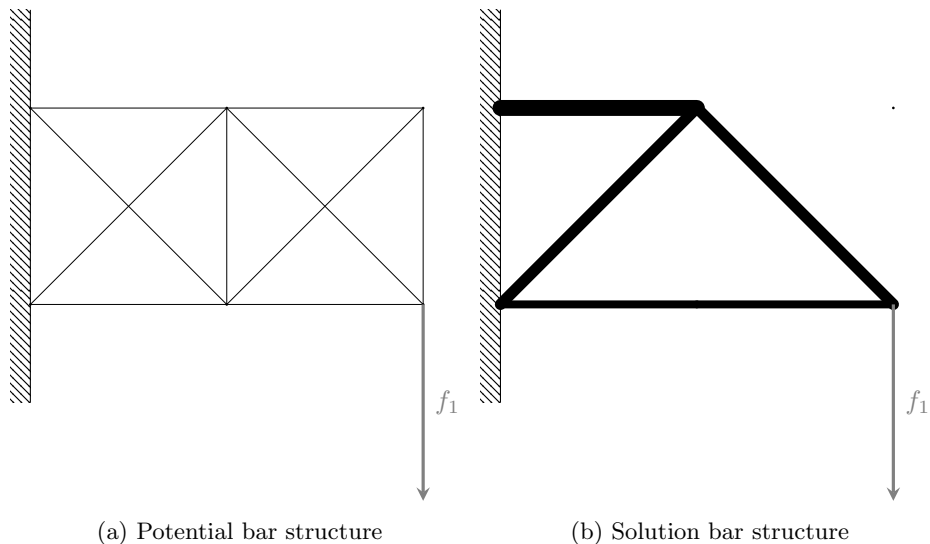


Figure 4: Potential bars and solution of the `TenBar` instance, which visually coincide with e.g. [8, 11]. The load force f_1 is marked in dark grey. On the left the structure is fixed on the grey wall.

Table 2: Results of the **TenBar** instance for the controlling constraints a_i , the stress values σ_i , the displacement variables u_j . We also show the compliance $f_1^T u$ and optimized Volume V^*

i	a_i^*	$\sigma_i(a^*, u^*)$	j	u_j^*
1	1.00000	-1.00000	1	-1.00000
2	1.41421	-1.00000	2	-2.72241
3	2.00000	1.00000	3	1.00000
4	0	0.86120	4	-3.00000
5	0	-0.27758	5	-2.00000
6	1.00000	-1.00000	6	-8.00000
7	0	-0.91333	7	1.47111
8	0	0.47111	8	-7.02019
9	1.41421	1.00000	$f_1^T u = 8.00000$	
10	0	0.97980	$V^* = 8.00000$	

6.2.2 Cantilever Problem

The next, more challenging truss design problem consists of the design of a cantilever arm. The instances, shown in Figure 5a, consist of 27 points placed in three rows. Once again, the leftmost points are attached to a wall, while a loading force pointing downwards is applied to the rightmost node on the bottom. Potential bars are present between all pairs of points where long bars overlapping shorter ones are removed. To this end, we let $(x_i, y_i) \in \mathbb{N}^2$ be (integer) coordinates of the points, noting that the bar between points i and j is overlapping if $\gcd(x_i - x_j, y_i - y_j) \neq 1$. Consequently, potential bars are present for 224 of the 351 pairs of points. Following [8], We consider three parameter sets $\bar{a} = 100$, $c = 1.0$, $\bar{\sigma} \in \{2.2, 100\}$, yielding the instances **Cant1** and **Cant2**.

The solutions, depicted in Table 3 are similar to those of the previous instance, where convergence is achieved within less than 20 iterations and 1287 to 3228 **Ipopt** Iterations. The computation time however differs widely between the instances, depending on the choice of scaling. As can be seen from the final configuration, several vanishing constraints become active in **Cant2a** and **Cant2b**, and several branches have to be explored until a solution is found, increasing the number of iterations, but not necessarily run times. Conversely, for **Cant1** no VC is in the lower branches at the solution, coinciding with the results in [8].

In Figure 6 we also present two solutions for instance **Cant2** in order to show that small differences in the method can lead to a different local solution. We therefore divide the instance **Cant2** into two subinstances. In instance **Cant2a**, we use the algorithmic parameters as they are. In instance **Cant2b**, the scaling of the variables is turned off and, at the same time, the scalar products for the primal variables and slack variables as described in (3) are changed from the Euclidean scalar products to the scalar products with absolute values of

the primal Lagrange gradient of (MPVCS) on the diagonal and added value of ρ . The solutions of **Cant2a** and **Cant2b** differ and is a typical behaviour of vanishing constraint problems caused by their non-convex feasible set. Although fewer bars are required for the truss structure, the volume of 30.63 in **Cant2b** is higher than the volume of 23.9741 in **Cant2a**. At the same time, more Ipopt iterations are required, which leads to a longer runtime for instance **Cant2b**. The results are noted in Table 3.

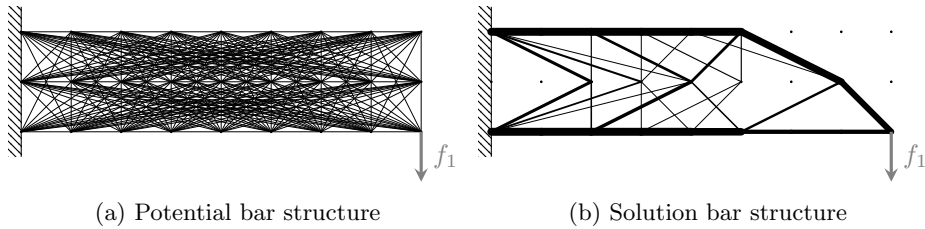


Figure 5: Potential structure of the cantilever problem in (a) and the solution of the **Cant1** instance in (b). The load force f_1 is marked in dark grey. The structure is fixed to the wall on the left-hand side.

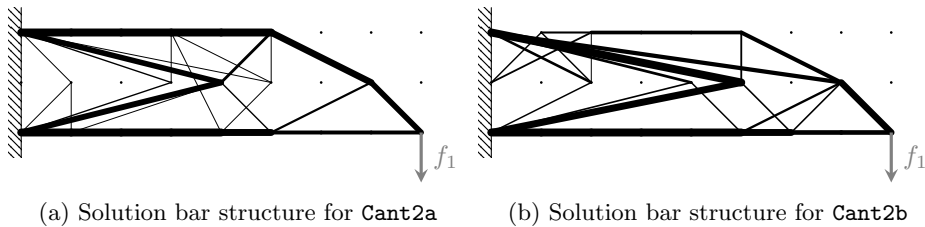


Figure 6: Influence of scaling on instance **Cant2**: Scaling of variables in (a) and not in (b), without scalar product scaling in (a) and primal and slack variable scalar product scaling based on the Lagrange gradient and parameter ρ in (b).

6.2.3 Hook Problem

The final problem, again described in [8], is called the *hook problem* owing to the shape of the structure as depicted in Figure 7a consisting of 35 nodes. The structure is attached at its top with a load being applied to a node at its far right. All nodes once more have integer coordinates, enabling us to detect overlapping potential bars as before, resulting in a total of 661 potential bars. We consider three parameter sets $\bar{a} = 100$, $c = 100$, $\bar{\sigma} \in \{3, 3.5, 100\}$.

The detailed solutions are listed in Table 3 and visualized in Figure 7. In **Hook1**, the first parameter set with $\bar{\sigma} = 100$ is used. It can be observed that, as in [8], the stress constraint is not active. The structure forms a half-circle open at the top (see Figure 7b). With 21 bars, there are significantly fewer bars than in [8], which can be related to the single load case.

The problem instance `Hook2` attains the maximal stress of $\bar{\sigma} = 3.5$, which turns active during the optimization but not in the solution, leading to the same structure with the same volume of 9.1118. These results of `Hook1` and `Hook2` illustrate the influence of the parameter $\bar{\sigma} = 3.5$, as reflected in the shorter run time, different maximal stress, and iteration numbers. In `Hook3` we further decrease the $\bar{\sigma}$ to 3.0. Again, the solution bar structure consists of 21 bars showing the same structure as `Hook1`, but, the maximal stress value for solution bars $\hat{\sigma}_{\max} = 3.0$ is active. The volume has increased to 10.0691. The number of vanished constraints again increases with the decreasing of $\bar{\sigma}$, i.e., we have constraints in the lower branch C_0 . The shorter run time is surprising and is a result of the lower number of iterations of both our approach and the subproblem solver `Ipopt`.

Lastly, owing to the larger problem sizes, the computation time increases significantly approximately one to three hours for the instances compared to the cantilever instances. However, the number of iterations of our approach remains roughly small. Thus, progress towards convergence is impeded by the increase in time required to solve the individual subproblems.

Table 3: Detailed solutions of listed problem from Table 1 showing the optimal volume V^* , the numbers of resulting bars, the maximal stress values σ_{\max} and the maximal stress value for solution bars $\hat{\sigma}_{\max}$ (i.e., $a_i > 0$), the configuration between lower branches ($\#C_0$) and upper branches ($\#C_+$), the number of iterations, the overall number of `Ipopt` iterations, and the computation time in seconds.

Problem	V^*	#bars	σ_{\max}	$\hat{\sigma}_{\max}$	$\#C_0 \#C_+$	#it	ipopt#it	time [s]
TenBar	8.0000	5	1.0	1.0	0 10	7	181	0.40
Cant1	23.1399	37	2.78132	2.78132	0 224	13	1287	395.08
Cant2a	23.9741	32	3.08450	2.20000	18 206	14	1013	318.86
Cant2b	30.6300	30	7.39528	1.81591	2 222	18	3228	949.15
Hook1	9.1118	21	7.21085	3.31283	0 661	14	2968	11237.90
Hook2	9.1118	21	3.49038	3.31282	0 661	18	1767	6928.56
Hook3	10.0619	21	5.19010	3.00000	8 653	12	787	3288.61

6.2.4 Comparison to Relaxation Approach

We compare the results with the calculations of the relaxation approach from [8]. For truss topology design problems, this is:

$$\begin{aligned}
& \min_{a \in \mathbb{R}^N, u \in \mathbb{R}^{Ld}} \sum_{i=1}^N \ell_i a_i \\
& \text{s.t.} \quad K(a)u_l = f_l && \text{for all } l = 1, \dots, L \\
& \quad \quad f_l^T u_l \leq c && \text{for all } l = 1, \dots, L \\
& \quad \quad 0 \leq a_i \leq \bar{a} && \text{for all } i = 1, \dots, N \\
& \quad \quad r_{il}^t(a, u) \geq -t && \text{for all } i = 1, \dots, N, l = 1, \dots, L.
\end{aligned}$$

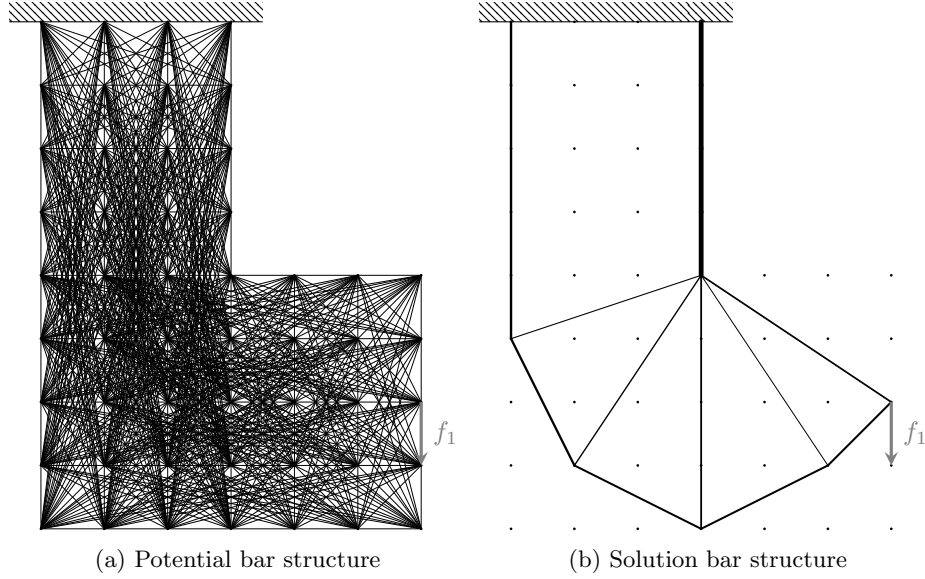


Figure 7: Potential and solution bar structure of Hook1, Hook2, and Hook3

Where t is the *relaxation parameter* and

$$r_{il}^t(a, u) := \varphi^t(a_i, \bar{\sigma}^2 - \sigma_{il}(a, u)^2) \quad \text{for all } i = 1, \dots, N, l = 1, \dots, L, \text{ with}$$

$$\varphi^t(w, v) := \frac{1}{2} \left(wv + \sqrt{w^2v^2 + t^2} + \sqrt{v^2 + t^2} - v \right).$$

The results are presented in Table 4. The computation times whenever a solution is obtained was around ten times faster. Consistent with the observations in [8], we achieve convergence for the instances **TenBar** and **Cant1** using the relaxation parameter of $t = 10^{-2}$. Note the importance of selecting an appropriate value of t , otherwise **Ipopt** aborts with maximal iterations reached or restoration failed messages (marked with DNF in Table 4). For instance, in **hook1** it can be observed that convergence is not achieved, even when different relaxation parameters are applied. Figure 8 shows representative outputs from the relaxation approach.

Figure 8a displays the optimal solution of **Cant2** for a relaxation parameter of $t = 10^{-3}$, which is structurally consistent with our flow approach solution for **Cant1** and the results from [8]. The volume is slightly smaller with a value of 22.8013 compared to all cantilever instances computed with our approach. The overall iterations of **Ipopt** are less in the relaxation approach. Figures 8b and 8c depict the outputs for **Hook1** obtained with relaxation parameters $t = 10^{-2}$ and $t = 10^{-5}$, respectively. The first output is a feasible structure similar to our gradient-flow solution of the hook instances, but with a larger volume of 9.19915 and 18 bars. The second output is an infeasible point and shows how different the last iteration of the solver can look like.

Unfortunately, we were unable to reproduce the same local minima found in [8]. Due to the non-convexity of vanishing constraint problems, it is not surprising that the results are not always fully correspond with previous calculations. In contrast, our gradient-flow approach successfully solves all listed instances. However, if only an approximation is required and a suitable relaxation parameter exists, the relaxation approach can save a considerable amount of computation time, but having the risk only to converge to feasible points.

Table 4: Detailed solutions of the relaxation approach with varying relaxation parameter t . We denote the iteration number of Ipopt [23], if it the solver printed the message 'Optimal solution found'. Otherwise we write DNF as short for did not finish.

Value of t	10^{-2}	10^{-3}	10^{-4}	10^{-5}	10^{-6}	10^{-7}	10^{-8}	10^{-9}
TenBar	34	156	DNF	DNF	46	66	53	DNF
Cant1	690	982	DNF	DNF	DNF	DNF	DNF	DNF
Cant2	DNF	571	541	DNF	DNF	DNF	DNF	DNF
Hook1	DNF							

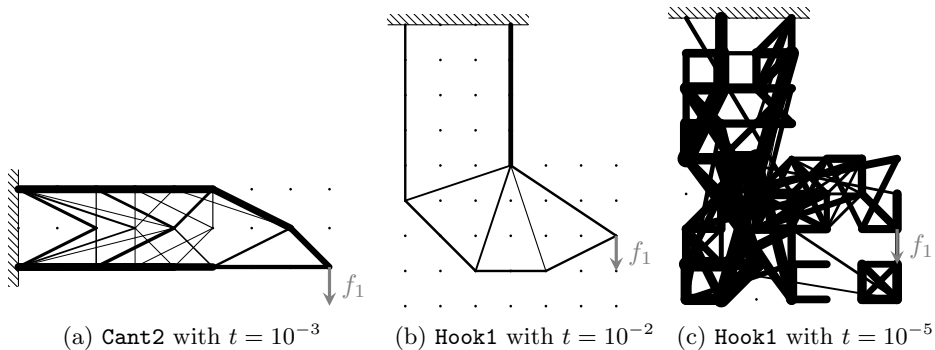


Figure 8: Different bar structures of Cant2 and Hook1 with different relaxation parameters. In (a) we show an optimal solution. In (b) and (c) we see the output of the not finished optimizations of Hook1.

7 Conclusion and Future Work

This work offers a novel approach for computing strong stationary points in Mathematical Programs with Vanishing Constraints (MPVCs). The proposed method exploits the problem structure via a slack-variable formulation of vanishing and controlling constraints, systematically selecting and switching between convex subsets of the slack-variable feasible set. This approach allows to keep track of the primal-dual gradient/anti-gradient flow at each iteration through

the solution of a convex subproblem. Since these subproblems can be solved using standard optimization solvers, our approach improves practical applicability. Numerical experiments on truss topology design problems with a single load case demonstrate the effectiveness of the proposed gradient flow approach, which outperforms a compared standard relaxation method.

Acknowledgements

Supported by the German Federal Ministry of Research, Technology and Space (BMFT) under Grant No. 05M22VHA.

References

- [1] Wolfgang Achtziger and Christian Kanzow. “Mathematical programs with vanishing constraints: optimality conditions and constraint qualifications”. In: *Mathematical Programming* 114 (2008), pp. 69–99. DOI: 10.1007/s10107-006-0083-3.
- [2] Joel A E Andersson, Joris Gillis, Greg Horn, James B Rawlings, and Moritz Diehl. “CasADi – A software framework for nonlinear optimization and optimal control”. In: *Mathematical Programming Computation* (2018).
- [3] Martin Philip Bendsoe and Ole Sigmund. *Topology optimization: theory, methods, and applications*. Springer Science & Business Media, 2013. ISBN: 978-3642076985.
- [4] Matúš Benko and Helmut Gfrerer. “An SQP method for mathematical programs with vanishing constraints with strong convergence properties”. In: *Computational Optimization and Applications* 67.2 (2017), pp. 361–399. DOI: <https://doi.org/10.1007/s10589-017-9894-9>.
- [5] Michael L Flegel and Christian Kanzow. “Abadie-type constraint qualification for mathematical programs with equilibrium constraints”. In: *Journal of Optimization Theory and Applications* 124 (2005), pp. 595–614.
- [6] Monique Guignard. “Generalized Kuhn–Tucker conditions for mathematical programming problems in a Banach space”. In: *SIAM Journal on Control* 7.2 (1969), pp. 232–241.
- [7] Michael Hintermüller. “Semismooth Newton methods and applications”. In: *Department of Mathematics, Humboldt-University of Berlin* (2010).
- [8] Tim Hoheisel. “Mathematical programs with vanishing constraints”. PhD thesis. 2009.
- [9] Tim Hoheisel and Christian Kanzow. “On the Abadie and Guignard constraint qualifications for mathematical programmes with vanishing constraints”. In: *Optimization* 58.4 (2009), pp. 431–448.

- [10] Tim Hoheisel and Christian Kanzow. “Stationary conditions for mathematical programs with vanishing constraints using weak constraint qualifications”. In: *Journal of Mathematical Analysis and Applications* 337.1 (2008), pp. 292–310.
- [11] Tim Hoheisel, Blanca Pablos, Aram Pooladian, Alexandra Schwartz, and Luke Steverango. “A study of one-parameter regularization methods for mathematical programs with vanishing constraints”. In: *Optimization Methods and Software* 37.2 (2022), pp. 503–545. DOI: 10.1080/10556788.2020.1797025. URL: <https://doi.org/10.1080/10556788.2020.1797025>.
- [12] Alexey F Izmailov and Mikhail V Solodov. “Mathematical programs with vanishing constraints: optimality conditions, sensitivity, and a relaxation method”. In: *Journal of Optimization Theory and Applications* 142.3 (2009), pp. 501–532.
- [13] Christian Kirches, Andreas Potschka, Hans Georg Bock, and Sebastian Sager. “A parametric active set method for quadratic programs with vanishing constraints”. In: *Technical Report* (2012).
- [14] Zhi-Quan Luo, Jong-Shi Pang, and Daniel Ralph. *Mathematical programs with equilibrium constraints*. Cambridge University Press, 1996. ISBN: 978-0521-572-903.
- [15] *MacMPEC, A collection of Mathematical Programs with Equilibrium Constraints*. <https://wiki.mcs.anl.gov/leyffer/index.php/MacMPEC>.
- [16] Olvi L Mangasarian and Stan Fromovitz. “The Fritz John necessary optimality conditions in the presence of equality and inequality constraints”. In: *Journal of Mathematical Analysis and applications* 17.1 (1967), pp. 37–47.
- [17] Robert Mifflin. “Semismooth and semiconvex functions in constrained optimization”. In: *SIAM Journal on Control and Optimization* 15.6 (1977), pp. 959–972.
- [18] Jorge Nocedal and Stephen J. Wright. *Numerical Optimization*. Springer New York, 2006. ISBN: 978-0-387-30303-1.
- [19] Armin Nurkanović, Anton Pozharskiy, and Moritz Diehl. “Solving mathematical programs with complementarity constraints arising in nonsmooth optimal control”. In: *Vietnam Journal of Mathematics* (2024), pp. 1–39.
- [20] Andreas Potschka and Hans Georg Bock. “A sequential homotopy method for mathematical programming problems”. In: *Mathematical Programming* 187.1 (2021), pp. 459–486.
- [21] Holger Scheel and Stefan Scholtes. “Mathematical programs with complementarity constraints: Stationarity, optimality, and sensitivity”. In: *Mathematics of Operations Research* 25.1 (2000), pp. 1–22.
- [22] Stefan Scholtes. “Convergence properties of a regularization scheme for mathematical programs with complementarity constraints”. In: *SIAM Journal on Optimization* 11.4 (2001), pp. 918–936.

- [23] Andreas Wächter and Lorenz T Biegler. “On the implementation of an interior-point filter line-search algorithm for large-scale nonlinear programming”. In: *Mathematical programming* 106.1 (2006), pp. 25–57. DOI: 10.1007/s10107-004-0559-y.